ADVANCED FUNCTIONAL MATERIALS
www.afm-journal.de

Bioinspired Directional Surfaces for Adhesion, Wetting, and Transport

*Matthew J. Hancock, Koray Sekeroglu, and Melik C. Demirel**

In Nature, directional surfaces on insect cuticle, animal fur, bird feathers, and plant leaves are composed of dual micro-nanoscale features that tune roughness and surface energy. Here, experimental and theoretical approaches for the design, synthesis, and characterization of new bioinspired surfaces demonstrating unidirectional surface properties are summarized. The experimental approaches focus on bottom-up and top-down synthesis methods of unidirectional micro- and nanoscale films to explore and characterize their anomalous features. The theoretical component focuses on computational tools to predict the physicochemical properties of unidirectional surfaces.

1. Introduction

In the plant and animal kingdoms, directional textured surfaces with microscale and nanoscale features provide key functions for survival.[1] Directional surfaces enable butterflies to cast water from their wings, water striders to walk on water, and plants to trap pollen and insects. Directional textured surfaces on gecko, spider, and lizard feet allow the animals to climb smooth and rough vertical walls, which requires that they controllably adhere to and detach from smooth and rough surfaces. The intestine and the lung are lined with microvilli that direct flow. All these natural surfaces derive their directional properties from asymmetric micro- or nanostructures such as ratchets or hairy forests, the asymmetric placement of such structures, or an emergent property due to a surface being coated with many copies of such structures. At the macroscopic scale, directionality manifests itself as anisotropic or unidirectional materials or processes. By contrast, at the molecular scale, thermal Brownian motion and molecular polarity fuel spatial or dynamical symmetry breaking. A system exhibiting such directionality is often called a molecular ratchet.[2]

Inspired by natural directional surfaces, engineers have developed a myriad of synthetic surfaces with precisely tuned physicochemical properties to transport water droplets and soft materials, control liquid spreading, provide directional adhesion and exhibit directional friction. Due to the wide range of applications, there has been an increasing interest in studying the anisotropy of biological and synthetic materials. Reviews already exist for the large body of research on natural[3,4] and engineered[5] superhydrophobic surfaces including the water repellent hairy exteriors of plant and animal species. Another review highlighted methods for synthesizing materials for dry adhesion that mimic the lizard or insect footpads.[5] This article focuses on anisotropic wet and dry adhesion properties of surfaces from experimental and theoretical perspectives. We first define anisotropy in Section 2 and then characterize the myriad of directional biological surfaces in Section 3. In Section 4, we review existing synthetic directional nanofilms and their applications. Finally, in Section 5, we outline theoretical approaches for modeling wet and dry adhesion on materials demonstrating unidirectional surface properties.

2. Definition of Anisotropy in Materials Science

The physicochemical properties of materials often depend on direction. Most materials have anisotropic physical properties because of their asymmetric micro- and nanoscale features. To determine the anisotropy of a system, a host of factors must be considered: the asymmetry of the material's structure and geometry; the asymmetry of the external field or stress; the asymmetry of the surface or boundary conditions; the asymmetry of the physical property relating stress to strain; and the asymmetry of the resulting body motion or deformation. These anisotropic factors are described schematically in **Figure 1**. Here the stress and strain could be external (e.g., mechanical, optical, electrical, or magnetic) or internal (e.g., self-oscillatory chemical reactions[6]). Examples include the walking of an asymmetric gel strip fueled by an oscillating chemical reaction (i.e., Belouzov[7]–Zhabotinsky[8]) and a polymer-magnetic composite swimmer actuated by a magnetic field.[9] Figure 1a illustrates types of material asymmetries, which could be due to structural or compositional variations. A recent review on nanomaterials assembly classified these variations in detail.[10] An example of material asymmetry is the class of anisotropic superstructures formed by uniformly amphiphile-coated spherical nanoparticles to balance the energy gain between particle coalescence and the entropy of the distorting grafted polymers.[11] A schematic of field asymmetry is shown in Figure 1b; a particular example is the anisotropic lateral vibration on a hydrophobic surface that induces unidirectional drop motion.[12] The influence of boundary conditions and geometry is illustrated in Figure 1c. The material itself may be isotropic, but its behavior

Dr. M. J. Hancock, K. Sekeroglu, Prof. M. C. Demirel
Materials Research Institute
The Pennsylvania State University
University Park, PA 16802 USA
E-mail: mdemirel@engr.psu.edu

DOI: 10.1002/adfm.201103017

may be anisotropic due to, for example, surface texture. Also, anisotropy may arise from multibody and single body interactions. In many cases, the asymmetric nature of a material is the result of a many-body emergent property. For example, a forest of carbon nanotubes[13] or a textured polymer nanofilm[14] will have different mechanical responses than the individual nanotubes or fibers. The most commonly known anisotropy of materials systems is sketched in Figure 1d: an anisotropic stretch or contraction can be created if the modulus has internal asymmetry. Lastly, strain asymmetry is illustrated in Figure 1e. An example is Purcell's swimmer,[15] made of three slender rods, that performs an asymmetric stroke to translate at low speeds in viscous fluids.

3. Examples of Directional Surfaces in Nature

Directional surfaces composed of asymmetric structures are widely used in Nature for wet and dry adhesion (**Figure 2** and **Table 1**).[16] Some insects employ a special form of wet adhesion by secreting adhesive fluids through arrays of setae to adhere to smooth or rough substrates. The beetle uses such a technique to respond to a disturbance by activating a tarsal adhesion mechanism,[17] which collectively bears approximately 60 000 directionally adhesive bristles (Figure 2a). While defending itself from a predator, the beetle presses a surface with all its bristles to withstand pulling forces of up to 60 times its body mass for up to 2 min.[17]

The hairy appendages of lizards, geckos and spiders have extremely fine endings[25] and finer adhesion structures to allow these creatures to climb both smooth and rough vertical surfaces via dry adhesion.[26,27] The flexible hairs on such appendages bend and allow a much greater contact area with uneven surfaces compared to smooth appendages, a mechanism called "contact splitting".[26,27] The density of hairs on such appendages scales with body mass.[27] Insects, for example, have lower hair densities compared to lizards. Autumn et al.[25] reported the first direct measurements of the force on a single seta of a gecko toepad by using a two-dimensional micro-electromechanical system. The many fine terminal endings of a single seta as well as the particular seta orientation produce attachment forces 600 times that compared to a smooth piece of the underlying material. In addition, the seta's directional structure (Figure 2b) allows the gecko toepad to be peeled from a substrate above a critical angle at a relatively low force compared with that of attachment. In many cases, a nanoscale thin film of adhesive fluid acts as a lubricating layer between the insect adhesive organs and the substrate.[28]

The ability of spider silk to collect water is an example of wet adhesion powered by a ratcheting mechanism (Figure 2c).[19] After wetting, a unique structure forms along a strand of spider silk. Periodic spindle-knots made of random nanofibrils are separated by joints made of aligned nanofibrils.[19] These directional structures create gradients in surface energy and Laplace pressure between the spindle-knots and joints, driving continuous condensation, and directional water drop collection about the spindle-knots.[19]

The directional surfaces on the wings and legs of insects play dynamic roles for thrust generation and drag reduction.[20] The remarkable non-wetting property of water strider legs is derived from their hierarchical hairy surfaces composed of numerous oriented needle-shaped microsetae with elaborate nanogrooves (Figure 2d).[21,29] A coherent view of the form and function of

Prof. Melik Demirel is a tenured associate professor in the Engineering Science and Mechanics Department and the Materials Research Institute at The Pennsylvania State University. Prof. Demirel's research focuses on understanding the anisotropic physicochemical properties of biological and synthetic materials. He received a Ph.D. in Materials Science and Engineering from Carnegie Mellon University (2002), and M.S. (1998) and B.S. (1996) degrees in Engineering from Bogazici University (Turkey).

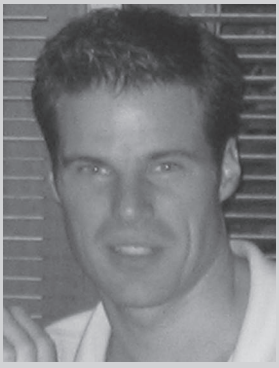

Dr. Matthew J. Hancock applies mechanics-based design, modeling, and simulation tools to biomedical engineering, medicine, materials science, and biology. He is currently a research fellow in Prof. Demirel's laboratory studying fluid transport on directional surfaces. Previously, he was a research fellow at Harvard Medical School and an instructor in mathematics at the Massachusetts Institute of Technology (MIT). He received bachelors and masters degrees in applied mathematics from the University of Waterloo, Canada, and a Ph.D. in environmental fluid mechanics from MIT.

Koray Sekeroglu is a Ph.D. candidate at Prof. Demirel's laboratory. His current research focuses on the fundamentals and physicochemical properties of directional polymeric films. He obtained his B.Sc in chemical engineering from the Izmir Institute of Technology in Turkey, where he subsequently worked as a research assistant.

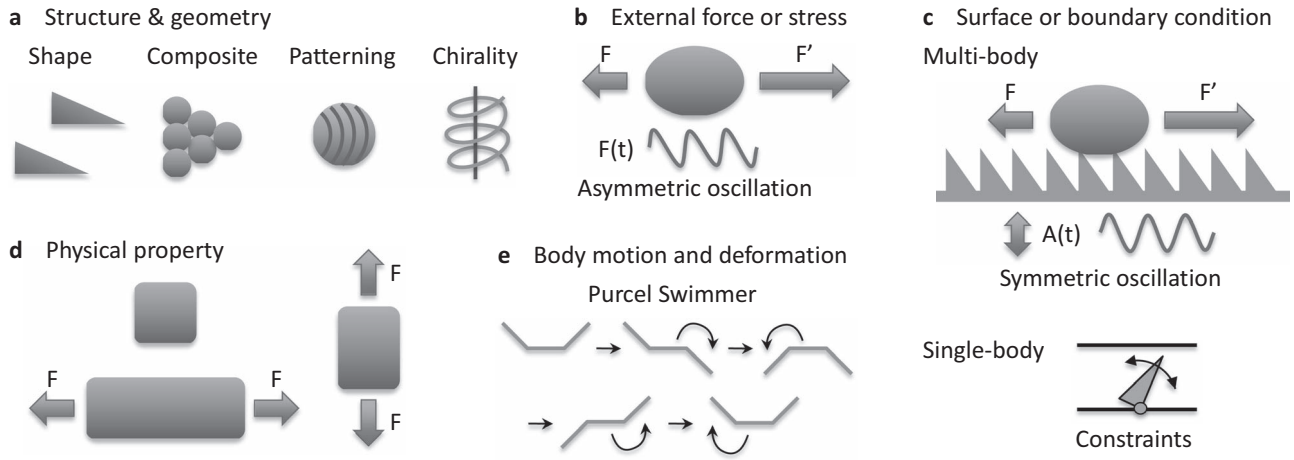

Figure 1. Sources of asymmetry in materials science. The asymmetry of a) the material's structure or geometry, b) the external field or stress, c) the surface or boundary conditions, d) the physical property relating stress to strain, and e) the strain or deformation.

the integument of water-walking insects and spiders was put forth in a recent review,[30] which demonstrated the influence of surface roughness on water repellency. Water repellency is a critical feature of water-walkers for avoiding entrapment at the interface, surviving the impact of raindrops, and submerged breathing. Butterflies have superhydrophobic wings composed of overlapping strips with directed flexible nanotips (Figure 2e).[22] A dew or rain droplet may slip off the surface of the wing in the direction away from the body, but is prevented from moving toward the body by the nanotips.

Directional surfaces are also common in the plant world. Pitcher plants have directional leaves that capture, retain, and

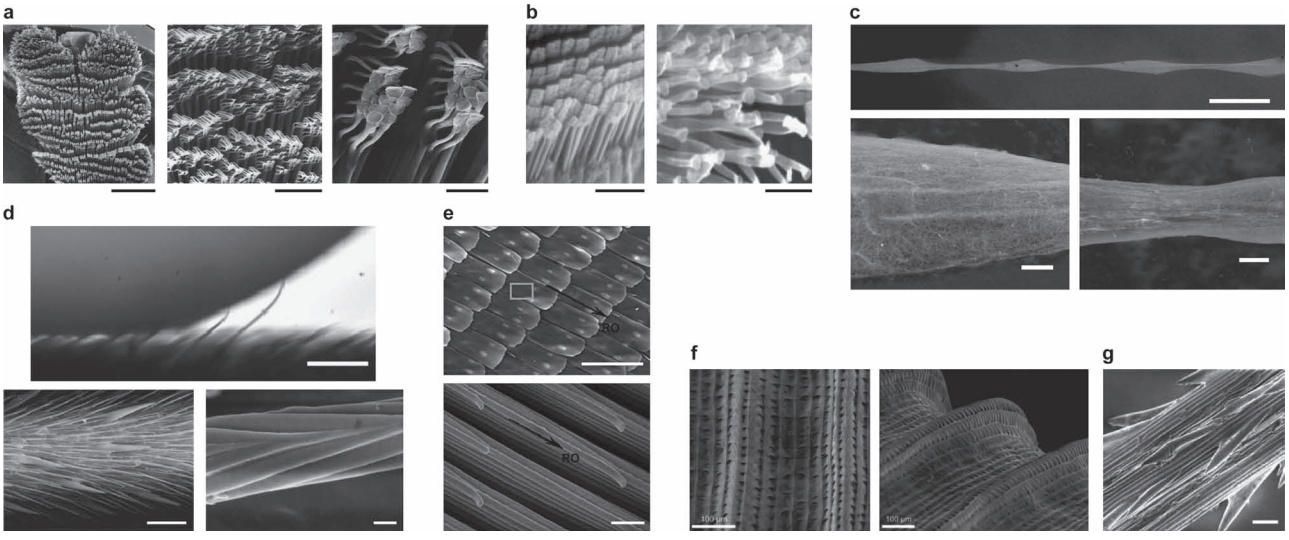

Figure 2. Directional textured surfaces in nature. a) Beetle (*Hemisphaerota cyanea*) tarsus consists of pads arranged in rows (left) and stuck together in clusters (middle, right). Scale bars, left to right, 200 µm, 40 µm, 10 µm. Reproduced with permission.[17] Copyright 2000, National Academy of Sciences, USA. b) Tokay gecko (*Gekko gecko*) foot setae (left) and the finest terminal branches of a seta, called spatula (right). Scale bars 50 µm (left) and 1 µm (right). Reproduced with permission.[18] Copyright 2000, Nature Publishing Group. c) Wet-rebuilt silk of the cribellate spider (*Uloborus walckenaerius*), showing overall structure (top) with environmental scanning electron microscope (ESEM) zooms of a spindle knot (bottom left) and joint (bottom right). Scale bars 50 µm (top) and 2 µm (bottom). Reproduced with permission.[19] Copyright 2010, Nature Publishing Group. d) The non-wetting leg of the water strider (*Gerris remigis*). Individual hairs are deflected by capillary forces as the drop advances against the grain (top). Scanning electron microscopy (SEM) images of the oriented microsetae (bottom left) and the nanoscale grooved structures on a seta (bottom right). Scale bars 100 µm (top), 40 µm (bottom left), 400 nm (bottom right). Top image reproduced with permission.[20] Copyright 2011, Elsevier. Bottom image reproduced with permission.[21] Copyright 2004, Nature Publishing Group. e) Overlapping microscales (top) on the wings of the butterfly (*Morpho aega*) are composed of aligned nanostripes. Scale bars 100 µm (top) and 400 nm (bottom). Reproduced with permission.[22] Copyright 2007, The Royal Society of Chemistry. f) Peristome surface of the *Nepenthes* pitcher plant has first and second order radial ridges. Scale bars 100 µm. Reproduced with permission.[23] Copyright 2004, National Academy of Sciences, USA. g) Microbarbs on the surface of the grass species *Hordeum murinum*. Scale bar 50 µm. Reproduced wtih permission.[24] Copyright 2009, The Royal Society.

Table 1. Characterization of directional textured surfaces.

Category	Figure examples
Structure	
hair/rod/groove	2a,b,d,g; 3a–k; 4a–c,e–g
scales	2e
surface contour	2c,f; 3l; 4h
multiscale	2a,b,d–f; 3k
Directional property	
dry adhesion	2b; 3i–k
lubricated adhesion	2a; 4d
wet adhesion	2c–f; 3a–h; 4a–c,e–f
mechanical force	2g; 4g
flow streamlines	3l
Usage	
water repellency	2d,e; 3a–c,e,f; 4b,c
water spreading	3d,g,h; 4a
transport	2c–f; 3a–c,e,f,l; 4b–e,h
adhesion	2a,b,g; 3i–k; 4g
Fabrication (engineered surfaces)	
template-free	3e,f; 4b,c,e–g
template-assisted	3j–l
lithographically patterned	3a–d,g–i; 4a,h

digest insects. Insect attachment is prevented on the plant's peristome by its anisotropic surface topography and by water lubrication (Figure 2f).[23] In another example, the anisotropic textured surfaces of grass awn naturally serve as motion rectifiers which convert non-equilibrium stresses from environmental sources such as variations in humidity into useful work (Figure 2g).[24] The ratchet efficiency is proportional to awn length and provides a selective environmental advantage to many plant species. Another example is the multi-length scale roughness that forms an anisotropic sliding surface on rice leaves.[31] Such natural surfaces have motivated the design and synthesis of a host of artificial directional surfaces.

4. Engineered Directional Surfaces: Form and Function

Inspired by the structure and utility of biological surfaces, a host of directional surfaces have been engineered with micro- and nanoscale features. Microscale surfaces with lithographically patterned asymmetric line patterns, posts, and textured walls have been engineered for transporting drops (**Figure 3**a–c and Table 1). The force of retention on a drop is less in the drop's direction of motion than in other directions. The source of this directional retention is related to contact angles and is discussed at length in the theory section (Section 5). A number of groups have created substrates with microposts arranged in periodic asymmetric patterns to induce droplet transport when the surface was mechanically vibrated or droplets were forced by oscillatory electric fields (Figure 3a).[32,33] Droplets have also been transported on microscale ratchet surfaces between parallel plates vibrated mechanically (Figure 3b).[34] The Leidenfrost effect,[35] in which a liquid or solid self propels on a hot surface, has also recently been employed to propel drops in a single direction on a hot ratchet surface (Figure 3c).[36] Lastly, surfaces patterned with asymmetric microstructures have controlled liquid spreading (Figure 3d).[37]

A number of nanostructured surfaces have recently been developed with directional wet adhesion properties. The advantage of using nanostructures is the tenfold or more increase in droplet retention forces over microstructured surfaces. Recently, we reported an engineered nanofilm composed of an array of hydrophobic PPX nanorods (poly-chloro-*p*-xylylene, a.k.a, parylene[46]), which is both hydrophobic and exhibits anisotropic wet adhesion via a ratchet mechanism (Figure 3e).[38] Such a nanofilm provides a microscale smooth surface for transporting microliter droplets. Another hydrophobic surface exhibiting anisotropic wet adhesion was composed of tilted nanostructures synthesized by ion track etching followed by a hydrophobic treatment (Figure 3f).[39]

Several groups have developed hydrophilic surfaces with nanoscale ratchets for controlled liquid spreading. Such surfaces could be used to channel fluids in microdevices for biosensing or liquid cooling applications. Replica molding and oblique electron beam irradiation were combined to create a surface with stooped polymer nanohairs to promote unidirectional spreading of a water droplet (Figure 3g).[40] Surfaces with tilted nanostructures may be designed to allow fluid to propagate in one direction while pinning it in all others (Figure 3h and **Figure 4**a).[41] Similar fabrication methods such as direct replica molding from a master with a slanted structure and nanofabrication (photolithography or molding) with post treatment such as electron-beam exposure, thermal annealing, and mechanical compression have been used to synthesize surfaces with tilted polymer nanorods for anisotropic wetting and directional dry adhesion.[5]

Inspired by the gecko footpad, surfaces have been engineered for directional dry adhesion. Examples include microfabricated wedge-shaped adhesive arrays[42] (Figure 3i) and vertically aligned arrays of angled microfibers (Figure 3j).[43] The latter synthetic angled microfiber array was prepared by a rolling process at 50 °C, which was lower than the glass transition temperature of the polymer. Yet another example is a nanofilm with hierarchical patterns of high aspect ratio polyurethaneurea-vinyl (PUA) rods formed over a large area from an etched polySi substrate patterned with tilted nanoholes (Figure 3k).[44] Our nanoPPX films also demonstrate directional dry adhesion.[51] By measuring the contact friction on these films, we found larger contact depths and higher friction coefficients for sliding in the direction of nanorod tilt compared to sliding against the tilt. In comparison, planar PPX films did not exhibit either frictional anisotropy or depth hysteresis.[51]

In addition to patterning planar surfaces, channels with asymmetric structures have also been engineered for directional transport applications. One of the first devices developed for transporting micron-sized particles employed a channel with ratchet-profile through which flow was periodically pumped (a single wavelength of such a channel is shown in Figure 3l).[45]

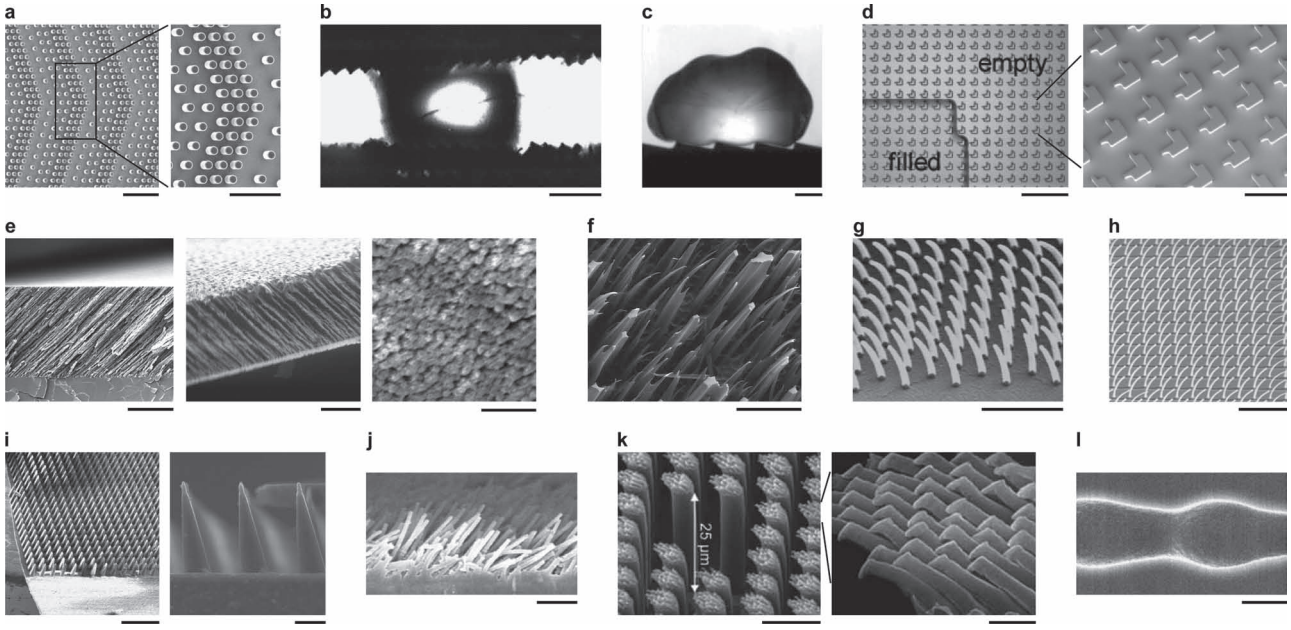

Figure 3. Engineered textured directional surfaces with asymmetric or periodic structures. a) Micropost array for directional drop transport. Zoomed image shows details of asymmetric positioning of posts. Scale bars 200 μm (left) and 100 μm (right). Reproduced with permission.[32] Copyright 2010, SPIE. b) Wax microratchet surfaces for directional drop transport. Scale bar 1 mm. Reproduced with permission.[34] Copyright 1999, the American Physical Society. c) Milliratchet surface for directional drop transport powered by the Leidenfrost effect. Scale bar 1 mm. Reproduced with permission.[36] Copyright 2011, Nature Publishing Group. d) Shaped micropillar array for directional droplet spreading. Scale bars 200 μm (left) and 50 μm (right). Reproduced with permission.[37] e) Nanofilm with tilted nanorods acting like nanoratchets for directional drop transport and adhesion. Scale bars 5 μm (left), 1 μm (middle, right). Reproduced with permission.[38] Copyright 2010, Nature Publishing Group. f) Ion track textured surface with directional contact angle hysteresis. Scale bar 50 μm. Reproduced with permission.[39] Copyright 2010, American Chemical Society. g,h) Tilted nanohairs for directional wetting and drop spreading. Scale bars (g) 1 μm and (h) 10 μm. Panel (g) reproduced with permission.[40] Copyright 2009, The Royal Society of Chemistry. Panel (h) reproduced with permission.[41] Copyright 2010, Nature Publishing Group. i) Microratchet surface for directional dry adhesion. Scale bars 500 μm (left) and 20 μm (right). Reproduced with permission.[42] Copyright 2009, The Royal Society. j) Tilted nanorods for directional dry adhesion. Scale bar 10 μm. Reproduced with permission.[43] Copyright 2008, American Institute of Physics. k) Hierarchical texture (micro/nano) for directional dry adhesion. Scale bars 10 μm (left), 1 μm (right). Reproduced with permission.[44] Copyright 2009, National Academy of Sciences, USA. l) Microchannel with ratchet-shaped walls for directional particle transport. Scale bar 2 μm. Reproduced with permission.[45] Copyright 2009, American Physical Society.

So far in this section we have focused on the structure of engineered directional surfaces. We now turn our attention to applications. The use of synthetic directional surfaces for dry adhesion applications has been reviewed earlier.[5] Here, we review applications of directional surfaces to soft materials (e.g., cells and gels) and liquids and augment the relatively few examples in the literature with new work from our group, including directional folding, friction, and transport (Figure 4 and Table 1).

Microfluidic devices require smart surface coatings for flow control. So far, such control has been achieved using chemical patterns[52,53] and topologically textured surfaces. The unidirectional surfaces described here may be patterned in microfluidic channels. The geometry of roughness elements, for example the tilt of nanorods, may be turned to achieve a particular fluidic resistance in continuous systems or contact line motion in drop-based (digital) systems. A preferential direction of transport may be achieved in a channel by aligning the unidirectional surface with the channel axis. Fluid droplets may either slide or roll on textured surfaces, depending on the viscosity, droplet size, wetting properties, and forcing characteristics.[12,54–56] Droplet motion may be powered by gravitational forces, alternating electric fields, or mechanical vibration.[12,54–56] Recent examples include unidirectional liquid spreading on nanofilms, where the liquid propagates in the tilt direction of hydrophilic nanoposts (Figure 4a),[41] and the unidirectional wetting behavior of hydrophobic nanofilms by a pin-release droplet ratchet mechanism (Figure 4b).[38,47] In the latter example, applying low-amplitude high frequency (≈30–80 Hz) vibrations on the boundary induced droplet transport in the direction the asymmetric asperities. The maximum droplet translation speed was approximately 3.5 mm s^{-1} and depended on both the drop volume and vibration frequency, discussed in detail in Section 5. By adjusting the vibration frequency, drops of different sizes could be selectively moved and merged.[47] Cargo such as microgels can be carried by such droplets (Figure 4b), which, combined with selective drop motion and merging, offers a pathway towards high throughput microgel assembly.[47]

Soft materials may also be transported on directional surfaces. One such example involves a gel cylinder riding atop a silicon rubber sheet (Figure 4d).[48] Angled parallel incisions were made in the rubber sheet, so that when vibrated, liquid seeped from the gel to form a thin lubricating layer between the gel and sheet. The asymmetric incisions opened only when the fluid between the gel and sheet sheared in one direction,

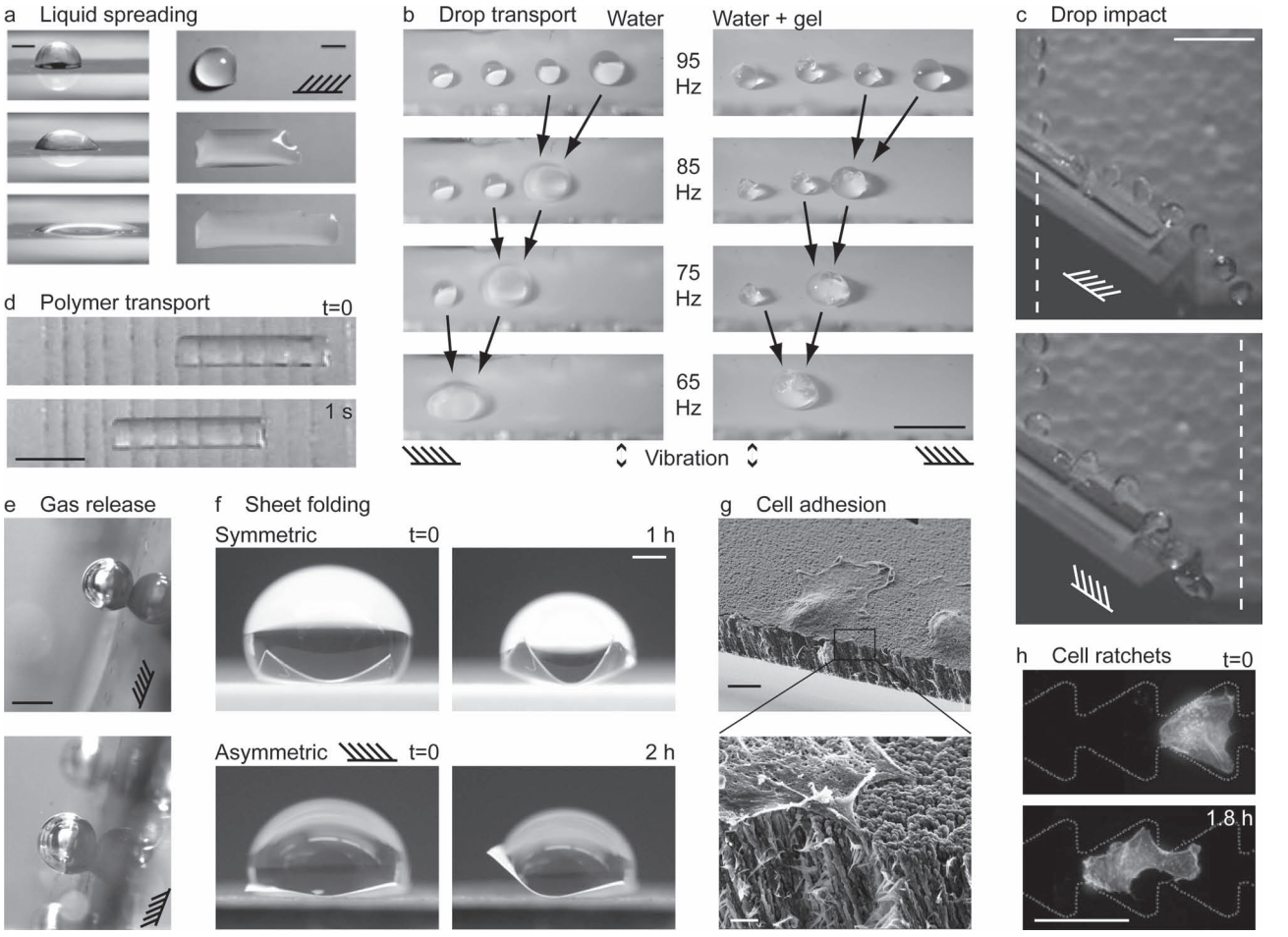

Figure 4. Applications of directional surfaces. a) Snapshots of a droplet spreading in one direction on a directional surface. Schematic indicates direction of nanorod tilt. Scale bars 1 mm. Reproduced with permission.[41] Copyright 2010, Nature Publishing Group. b) Drops and drops containing cargo being transported on directional surfaces forced with mechanical vibration. The forcing frequency was chosen close to the resonant frequency of the largest drop, and amplitude low enough so that smaller drops did not move. When two drops coalesced, their size increased and resonant frequency decreased. Thus, the forcing frequency was also reduced to keep the largest drop moving. Scale bar 5 mm. Reproduced with permission.[47] Copyright 2011, American Institute of Physics. c) Drops impacting a directional surface with the grain (top) bounce further than those impacting against the grain (bottom). Dashed vertical lines demark the extent of the trajectory in the top image; schematics indicate the grain, i.e., nanorod direction. Scale bar 1 cm. See Experimental Section for details. d) Soft gel transport on a PDMS surface with angled cuts aligned in the direction of motion. Snapshots shown 1 s apart. Scale bar 1 cm. Reproduced with permission.[48] Copyright 2004, National Academy of Sciences USA. e) Directional control of gas release. Gravity and buoyancy force act in (above) and against (below) the direction of nanorod tilt, as indicated by the schematic. Scale bar 1 mm. See Experimental Section for details. f) Directional folding. Polymer sheets were folded by evaporating droplets. Folding was symmetric and asymmetric for sheets with isotropic and directional surfaces, respectively. Scale bar 4 mm. See Experimental Section for details. g) Directional cell adhesion on a directional surface. Zoomed image indicates cell filopodia penetrating between the nanorods. Scale bars 10 μm (top) and 1 μm (bottom). Reproduced with permission.[49] Copyright 2011, American Vacuum Society. h) Channels with ratchet surfaces for cell transport. Scale bar 50 μm. Reproduced with permission.[50] Copyright 2009, Nature Publishing Group.

resulting in an asymmetric coefficient of kinetic friction and the gel being transported along the sheet.[48]

A rich class of phenomena arises when a droplet impacts a textured surface. For particular impact speeds, drops may rebound from superhydrophobic surfaces without actually wetting the surface.[57] For a unidirectional surface, we expect that contact line motion and the rebound trajectory will depend not only on impact speed, but also the angle of attack. Preliminary experiments performed at our lab showed that when drops impacted an inclined directional nanorod surface in the direction of nanorod tilt, the horizontal extent of the trajectory was larger than when drop impact was against the nanorod direction (Figure 4c). In addition to the rebound trajectory, we suspect that the critical impalement speed, rebound angle, and distorted drop shape will all depend on the orientation of droplet impact with respect to the asymmetric roughness features of the directional textured surface.

The directional release of gas bubbles may also be generated on anisotropic surfaces. We generated H_2 bubbles by the catalytic release from alkaline aqueous solutions of sodium borohydride on cobalt functionalized directional PPX matrices. Cobalt catalysts were prepared on PPX nanofilm substrates via electroless plating

with adsorbed pyridine ligand as an adhesion promoter.[58,59] The force of retention on gas bubbles was larger when the nanorods were pointing down than when pointing up (Figure 4e).

Capillary wrinkling and folding of thin sheets of soft material by droplets is another well documented phenomenon.[60] 2D soft polymer sheets will fold into 3D structures as a function of the number and direction of folds.[61] Anisotropic textured surfaces could control the directionality of a folding sheet by creating an asymmetry in the contact angles along the contact line of the water drop folding the sheet. In new preliminary experiments, we showed that the anisotropy of the nanoPPX can guide sheet folding (Figure 4f). Folding was driven by water evaporation following droplet deposition; the shrinking contact line of the evaporating droplet pulled the edges inward to drive the folding. The nanorod orientation determined the direction of folding: when the nanorod tilt was to the right, the receding contact angle along the right edge was smaller than that on the left, making the component of force larger on the right edge than on all other edges. Hence, the thin film bent to the left (Figure 4f).

Bioadhesion properties have also been observed on synthetic directional nanofilms,[49] making them potentially useful for tissue engineering applications. In a previous study, we used fluidic shear stress to remove cells from a microfluidic channel whose substrate was coated with our nanoPPX film (Figure 4g).[49] Cells were removed with lower shear stresses when the flow was in the direction of nanorod tilt, compared to flow against the tilt. Lastly, ratchet-like channel geometries have been shown to rectify the random motions of motile cells and induce cell migration along a channel (Figure 4h).[50]

5. Modeling Adhesion, Wetting, and Transport on Directional Surfaces

An integral part of understanding and designing directional surfaces involves modeling their behavior and interaction with fluids and solids. In this section we review an array of modeling approaches with a hierarchy of sophistication to model adhesion, wetting, and transport on directional surfaces. The five sources of anisotropy outlined in Section 2 and Figure 1 arise in theoretical models from asymmetries in the geometry or governing equations, such as conservation laws (i.e., mass, momentum, energy), kinematic relations, and constitutive equations with boundary conditions.[62] The salient anisotropic mechanism must be included in theoretical models to achieve accurate predictions. For example, simulations of the microtextures within metallic thin films agree well with experimentally characterized microtextures when anisotropic interface properties are incorporated in the calculations, while agreement is poor when isotropic properties are used instead.[63] Similarly, at the nanoscale, fluctuations about the native conformation of proteins have been suitably reproduced using an anisotropic network model, which enables evaluation of the directional preferences of proteins.[64]

5.1. Modeling Dry Adhesion

Models for dry adhesion are based on contact mechanics balancing elastic and surface energies and include crack-like mechanisms to model separation.[65] Contaminants or roughness reduce the strength of dry adhesion, while hierarchical structures can be used to increase it.[26,65] Modeling approaches range from analytic formulas to finite element method (FEM) simulations to calculate the contact mechanics in the presence of normal and shear loads between solids, viscoelastic material and biological matter.[18,25,65,66] A recent example is the contact mechanics-based analytic model used to elucidate the robust and releasable adhesion of the gecko foot.[65]

When a thin layer of lubricating liquid exists between two solids, additional fluidic forces must be coupled to the solid mechanical model to describe contact and adhesion. For the example outlined in Figure 4d (i.e., a gel cylinder transported on a polydimethylsiloxane (PDMS) layer with angled incisions), an analytic model was developed to describe the oscillations in the gel and its net motion.[48]

5.2. Modeling Wetting, Adhesion, and Transport in Solid-Fluid Systems

The wetting of solid surfaces by fluid and the adhesion and transport of fluid on solid surfaces depends on both the topology of the solid surface and the chemical and material properties of the fluid and solid phases.[30,67–69] In what follows, we provide a brief overview based on existing work[30,68] of two important concepts related to wetting, adhesion, and transport: contact angles and contact angle hysteresis. We then review theoretical tools for calculating and quantifying wetting, adhesion, and transport in solid-fluid systems. Though such tools have been applied mainly to isotropic surfaces, they may be readily generalized to directional surfaces. As reviewed below, thus far three groups have put forth models of wetting and adhesion on directional surfaces.[38,70,71]

The contact angle θ is defined as the angle measured through the liquid between the meniscus (liquid/gas interface) and the substrate (liquid/solid interface) at the three-phase (solid/liquid/gas) contact line. The equilibrium contact angle between a drop and a flat smooth surface is given by Young's relation,[72] $\cos\theta_e = (\gamma_{SG} - \gamma_{SL})/\gamma$, where γ, γ_{SL}, and γ_{SG} are the surface tensions of the gas/liquid, solid/liquid and solid/gas interfaces, respectively. In reality, a range of static contact angles, referred to as contact angle hysteresis, may be observed for a given solid-fluid combination,[73] $\theta_r \le \theta \le \theta_a$, bounded below and above by the receding and advancing contact angles. Contact angle hysteresis is directly related to adhesion because differences in contact angles around the drop perimeter can yield a net surface tension force that resists drop transport. The force of wet adhesion, also called the droplet retention force, is estimated by[74] $F_r = k\gamma R(\cos\theta_r - \cos\theta_a)$ where R is the radius of the drop and k is a coefficient depending on the shape of the contact line. Such a formula may be used to estimate the maximum force on a raindrop sticking to a window, where the advancing and receding contact angles θ_a and θ_r are the contact angles on the drop's lower and upper edges, respectively. Contact angle hysteresis is due to contact lines pinning on microscopic irregularities on the surface;[75] consequently, the most effective way to reduce it is by removing such irregularities via polishing, or conversely by minimizing the interaction between the interface and solid by roughening or texturing the surface.

On chemically heterogeneous or rough surfaces, the microscopic contact angle θ will generally differ from the apparent angle θ^* observed at a macroscopic scale. In cases where the fluid fully wets a rough surface, the apparent macroscopic contact angle θ^* is given by Wenzel's relation,[76] $\cos\theta^* = r\cos\theta_e$ where the roughness parameter r equals the real surface area per planar area of the surface. When air pockets are trapped between roughness elements and the liquid, θ^* is given by the Cassie–Baxter[77] relation, $\cos\theta^* = -1 + \varphi_s(1 + \cos\theta_e)$, where φ_s is the area solid fraction. The Cassie–Baxter formula reveals that as the area solid fraction vanishes, $\varphi_s \to 0$, the contact angle θ^* approaches 180°. For nanotextured surfaces, air pockets are trapped at the interface between water and nanoporous hydrophobic surfaces. Such air pockets may be generated when a hydrophobic surface is immersed in a liquid,[78] and may be quantified by X-ray scattering and contact angle measurements.[79] It has been shown that the layer of air at the solid-aqueous interfaces is less than 0.1 nm thick for several hydrophobic solids.[80]

5.2.1. Analytic Models of Contact Angle Hysteresis

An array of analytic models exist to predict contact angle hysteresis including simple averages of the intrinsic contact angles on a material surface and in the voids and scaling models incorporating the shape of the meniscus. Extrand's[81] geometrical scaling argument for the macroscopic advancing and receding contact angles, θ_a and θ_r, on a pillared substrate of a material with advancing angle over 90°, $\theta_{a0} > \pi/2$, gives $\theta_a = \pi$ and $\theta_r = \lambda\theta_{r0} + (1 - \lambda)\,\pi$, where λ is the linear solid fraction, defined differently for different types of configurations. For example, for square arrays, $\lambda = d/\delta$, where d is the post diameter and δ is the spacing. The contact angle hysteresis for a drop in a Cassie state on a pillared substrate has also been calculated[33] using a slice approach.[82] Other estimates have been made for the hysteresis on 2D substrates consisting of grooves with semicircular surface undulations and on 3D substrates consisting of pillars made up of many spheres.[83]

The hysteresis on more complicated surfaces such as fiber layers with regular or random spacing may be estimated using the more general framework of de Gennes and colleagues.[67,68,84–86] In the limit of small contact angle, the hysteresis for a flat surface with single and distributed chemical defects has been derived.[84] The word "defect" refers to a perturbation in the wetting energy localized near a particular point. The pinning argument has been repeated for $\theta = \pi/2$, i.e., a vertical meniscus on a flat surface passing a single chemical defect or a distribution of defects.[68] Similar results were found for the contact angle hysteresis due to weak random roughness.[85] The framework developed in these works may be used to determine the contact angle hysteresis of many textured surfaces, including directional surfaces.

Recently Reyssat and Quéré[86] generalized de Gennes' spring-like model to the case of a drop in a Fakir (Cassie) state on square array of cylinders. Assuming the resistance was due entirely to the receding contact line,[87] they calculated the force to depin the receding surface of the drop and found that the hysteresis scaled as the solid fraction φ_s times its log. Their model included a fitting parameter a quantifying the effects of contact line distortion: $\cos\theta_r - \cos\theta_a = (a\varphi_s/4)\log(\pi/\phi_s)$, where $a = 2$ (scaling) and $a = 3.8$ (data fit).[86]

We recently reported a simple ratchet model for the contact angle hysteresis to rationalize the directional wetting response observed in Figure 4b for the PPX nanofilm in Figure 3e.[38] The model was based on the directional dependence of the advancing and receding contact angles, θ_a and θ_r, of a sessile droplet on the tilted pillared substrate.[38] We estimated θ_a and θ_r by generalizing Extrand's[70,81] approach for 2D ratchets and 3D vertical pillars. Following Extrand, we introduced the linear fraction of the receding or advancing contact lines on the pillars, λ. The contact angles θ_r and θ_a were approximated as weighted averages, in terms of λ, of the respective contact angles between the meniscus and pillar and 180° in air. Simple geometrical arguments then provided estimates of the contact angle between the receding or advancing meniscus and the pillared substrate in terms of the intrinsic contact angles θ_{a0} and θ_{r0} of the substrate material, the pillar tilt angle β, diameter d, spacing δ, and the linear fraction λ.

A large class of the directional textured surfaces considered in Figure 2 and 3 consist of asperities with long and thin features that bend when in contact with droplets.[38] The tips of these flexible asperities can pull back on the trailing surface of the drop as it passes, enhancing hysteresis. A future goal is to integrate the effects of such flexibility into analytic models of contact angle hysteresis to improve predictions of wetting, adhesion, and transport.

5.2.2. Analytic Models of Drop Transport on Textured Surfaces

The relation between drop speed and vibration frequency, amplitude, drop volume, and surface parameters may be rationalized theoretically.[12,54–56] The power required to move a droplet at a speed U on a surface with retention force F_r scales as F_rU plus the rate of energy dissipation in the vibrating and translating drop. The retention force on a moving droplet is somewhat less than that for a static droplet, but the static calculation, proportional to contact angle hysteresis, gives a reasonable upper bound. Steady droplet motion is achieved when the energy transferred to the droplet is balanced by dissipation (e.g., Figure 4b). For drops with length scales smaller than the capillary length $l_c = (\gamma/\rho g)^{1/2}$, where ρ is fluid density and g is gravity, energy dissipation due to internal viscous motions is confined to a small dissipation zone near the region of contact with the substrate (elsewhere, the drop is in solid body motion) and scales as[55] $\mu U^2R^4/(l_c)^3$, where μ is the dynamic viscosity of the droplet fluid and R is the droplet radius. The dissipative losses due to vibration may be estimated from Stokes third problem[88] as $\mu k(a\omega)^2 l^2$, where $l \sim R^2/l_c$ is the radius of the contact region,[55] a and ω are the amplitude and angular frequency of vibration, and $k = (\omega\rho/2\mu)^{1/2}$. Drop speeds have been measured on isotropic textured surfaces for motion powered by gravity,[54,55] anisotropic mechanical vibration,[12] and on directional surfaces by mechanical vibration.[38,47] Drop speed is highly dependent on the forcing frequency. For the same input energy, larger drop speeds are associated with the Rayleigh modes of the droplet.[12,47] Estimates and scaling arguments of drop speed have been derived based on the simple estimates of contact angle hysteresis and dissipation listed above.[12,54–56]

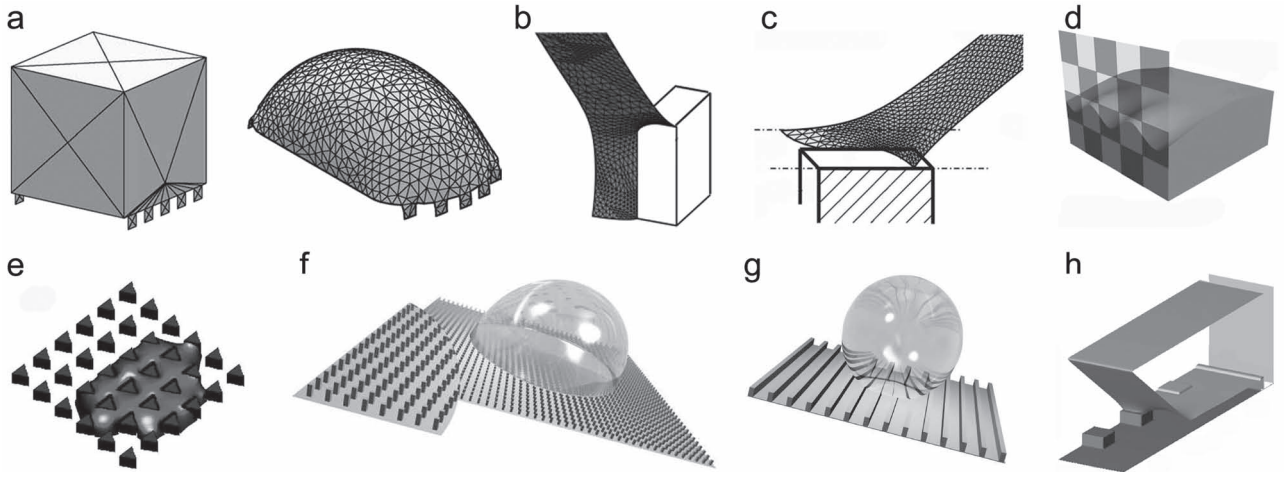

Figure 5. Modeling wet adhesion on textured surfaces. a) Initial and final Surface Evolver simulation profiles for a static drop on a pillared surface. Reproduced with permission.[93] Copyright 2005, Elsevier. b) Surface Evolver simulation of a portion of a droplet in a Wenzel state on a pillared surface. Reproduced with permission.[96] Copyright 2008, American Chemical Society. c) Surface Evolver simulation of a portion of a droplet in a Cassie state on a pillared surface. Reproduced with permission.[94] Copyright 2007, American Chemical Society. d) Surface Evolver simulation of a droplet advancing or receding on a checkerboard chemically patterned surface. Reproduced with permission.[92] Copyright 2010, American Chemical Society. e) Lattice Boltzmann simulation of directional spreading through an array of triangular pillars. Reproduced with permission.[99] Copyright 2009, Institute of Physics. f,g) Lattice Boltzmann simulations of drops sliding on pillared and grooved surfaces. Reproduced with permission.[100] Copyright 2007, Springer-Verlag. h) Lattice Boltzmann simulation of a portion of a drop in a Cassie state receding on a pillared surface. Reproduced with permission.[101] Copyright 2010, American Chemical Society.

5.2.3. Finite Element Models of Static Drops on Textured Surfaces

The simplest computational approach for modeling droplet behavior on textured surfaces involves FEM calculations of the static droplet meniscus and corresponding contact angle hysteresis. A popular public domain FEM package for such simulations is Surface Evolver,[89] which evolves a surface to achieve a state of minimal energy. The user creates an initial surface of vertices, edges, and faces and has broad control over the mesh refinement, surface evolution, energy functionals, and convergence. The initial surface is iteratively evolved and refined until a local energy minimum is reached (**Figure 5**a). The package also includes basic programming constructs such as loops and conditional statements. Surface Evolver has been used to calculate free surface profiles on isotropic surfaces with chemical patterns,[52,90–92] parallel grooves,[93] pillars,[94–96] (Figure 5b,c) and inverted pillar surfaces.[97] Surface Evolver has also been used to calculate droplet profiles in electric fields.[98]

To calculate the contact angle between a sessile drop and a rough surface, the size of the computational domain may be significantly reduced when the roughness scale is much smaller than the drop radius and the capillary length (Figure 5b,c). In this regime, a good approximation is that the curvature of the liquid/gas interface near the roughness is effectively zero compared to the scale of the roughness. A zero curvature constraint may then be imposed within Surface Evolver to simulate the meniscus near the asperities. Note that zero curvature does not imply a planar geometry; a saddle shape in which the component curvatures in perpendicular directions cancel also has zero curvature. Such saddle-like topology characterizes the meniscus geometry near the contact line of a drop on a rough surface. However, at the scale of the roughness, the far field condition (away from the roughness) is that the receding surface is in fact planar. In this regime, using such an approach allows the shape of the three-phase contact line and the local contact angle to be calculated to a good approximation with a computational domain that includes only the nearby free surface, and not the entire drop surface. Symmetries in the roughness configuration may also be used to further reduce the size of the computational domain.[94,96]

The key to modeling adhesion and transport is to move beyond calculations of contact angles to the limiting cases of advancing and receding angles. In one of the few studies to report such a calculation, Kwon et al.[92] calculated the advancing and receding angles by gradually increasing or decreasing the volume of a drop, respectively, on a chemically patterned surface and averaging the contact angle along the contact line just prior to depinning events (Figure 5d). When the contact line moved, local contact angles were enforced by a phase field model coupled to the Surface Evolver calculations. The concept of coupling the phase field model to the FEM simulations not only maintained accurate contact angles during contact line motion, but also allowed the intrinsic advancing and receding angles of the material to be included in the simulations. Such an approach could be extended to model contact angle hysteresis for surfaces with hierarchical scales of roughness, such as those of the Lotus leaf.

The previous contact angle hysteresis models, both analytic and finite element, have all calculated the static meniscus. As noted above, the static calculations are useful to provide upper bounds on the wet adhesive property of a surface. However, accurately modeling dynamic situations such as a drop sliding

along a surface or depinning events require full numerical treatment, discussed next.

5.2.3. Full Numerical Simulation of Free Surface Flows on Directional Surfaces

An array of numerical approaches exists to generate full dynamical simulations of free surface flows in and over complex geometries. At the microscopic scale, molecular-dynamics (MD) simulations have modeled contact line dynamics and shed light on wetting hysteresis due to chemical defects and roughness.[102] At the mesoscale, phase field models employ a free energy field variable that acts as a marker for the different continuum phases.[103] Phase field models have been used to model a variety of dynamic multiphase flow problems, including droplet hysteresis and contact line pinning and motion on chemically and structured heterogeneous surfaces.[103,104] Phase field models have been implemented with both sharp and diffuse treatments of the interface to model drop, free surface and contact line phenomena.[105] A popular phase-field diffuse-interface approach is the Lattice Boltzmann method (LBM).[106] In LBM, a mean-field lattice-gas cellular automata model is implemented with a set of distribution functions to represent the average population of fluid particles.[107] Free surfaces are implemented using a free energy functional that is minimized in equilibrium.[107] The model can be extended to complex and multiphase fluids and complex geometries. Thus, LBM is ideal for simulating chemically patterned and rough surfaces. An array of dynamic wetting problems have been solved including the spreading of a fluid through a post array (Figure 5e),[99] droplets sliding on inclined pillared and grooved substrates (Figure 5f,g),[100] periodic droplet formation within chemically patterned microchannels,[108] anisotropic adhesion on ratcheted surfaces,[71] the impalement of a droplet on a superhydrophobic textured surface,[109] the advancing of a meniscus through microchannels patterned by posts,[110] and receding contact lines on superhydrophobic surfaces (Figure 5h).[101] For static drops, FEM and LBM simulations produce comparable drop profiles.[91]

6. Conclusions

Inspired by directional surfaces in nature, engineers have employed recent innovations in microfabrication and materials synthesis to produce an array of synthetic directional surfaces with tunable anisotropic chemical, mechanical, physical, morphological, and topological properties. Such directional surfaces may exhibit a host of emergent properties such as friction and wetting. These directional surfaces not only mimic biological surfaces, but also provide new avenues to discover surface phenomena beyond those in nature. In concert with innovative synthesis techniques, theoretical and computational tools link the structure to the behavior of directional surfaces. The next generation of directional surfaces will find use in syringes, hydropower turbines, micro- and nanoscale microfluidic devices for biomedical research, drag reducing and non-fouling ship hull coatings, self-cleaning solar-cell panels, high-efficiency thermal cooling systems for microchips, and friction-control coatings for tires.

A future challenge is to engineer dynamic directional surfaces that change wetting and friction properties in real-time and enact such changes in response to external stimuli. In Nature, various stimuli-response mechanisms exist to modify the surface shape or wetting properties. For example, water striders release surfactants to break through the free surface while laying eggs.[3] Certain insects generate emergency propulsion by releasing surface-active fluids to generate Marangoni stresses.[3] Many surface dwelling insects lift or pierce the free surface using retractable wetting claws at the ends of their hydrophobic legs.[111] Inspired by these natural systems, engineered surfaces exist that change their wetting and adhesion properties on command or in response to stimuli.[112] Such systems also employ surface clumping to lower the surface solid fraction and temperature gradients to induce surface tension gradients. Under the right conditions, cycling the stimulus may induce transport, offering a method to propel cargo or droplets in addition to mechanical vibration, acoustics, and electrowetting. Marangoni flows induced by surfactant release could also be used to create fluid motion on a unidirectional surface. New theoretical tools must also be developed to link the structure and stimuli response mechanisms to the overall behavior of the directional surface and to better inform design criteria for optimal behavior.

7. Experimental Section

Asymmetric and Symmetric Folding: Oblique angle polymerization (OAP) produced an array of parylene (PPX) nanorods on a substrate.[38] Commercial systems were used to produce the vaporization and pyrolysis of a *p*-cyclophane precursor to generate a diradical vapor flux. The flux was directed at a controlled shallow angle onto silicon substrate, where surface diffusion combined with deposition geometry led to shadowing and selective growth of anisotropic structures during polymerization. The nanoPPX film (approximately 1 cm × 1 cm × 20 μm) was peeled off the silicon surface as a self standing film. PDMS films (approximately 1 cm × 1 cm × 30 μm) were prepared using Sylgard 184 Silicone Elastomer Base mixed at a 10:1 ratio with its associated curing agent. PDMS films were spin-coated on a silicon substrate, cured, and then lifted off the surface. Both films were placed on a hydrophobic surface with a contact angle of ≈130° to prevent adhesion of the film to the substrate.

Directional Bubbles: NanoPPX films were treated with 1 M pyridine (aq) for ≈48 h and rinsed in water for 4 min. The nanofilms were then immersed in a PdII-based colloidal dispersion for 45 min and were then rinsed in water for 1 min followed by plating for 1 min in a Co bath. The Co bath was prepared as previously described.[58,113] $NaBH_4$ solution in water was prepared using 2.5 wt% $NaBH_4$ (0.677 M) and 1 wt% NaOH(aq) solution (0.261 M). Finally, a cobalt coated nanoPPX film was dipped into the $NaBH_4$ solution for H_2 generation.

Drop Impact: NanoPPX films were coated on silicon substrates and placed on a 45° inclined support. A water drop of 10 μL was release from a height of 10 cm to the center of the nanofilm. The drop impact was recorded using a high speed camera (Redlake MASD PCI Motionscope) at an acquisition rate of 1000 fps and at a resolution of 128 × 128 pixels.

Acknowledgements

The authors gratefully acknowledge financial support for this work from the National Institutes of Health (1R21HL112114-01) and The Pennsylvania State University. The authors thank Dr. Benjamin Hatton

for helping with the high speed camera recordings for Figure 4c and Prof. John Bush for useful discussions and comments.

Received: December 13, 2011
Published online: March 13, 2012

[1] S. Vogel, *Life's Devices: The Physical World of Animals and Plants*, Princeton University Press, Princeton, NJ **1988**.
[2] P. Reimann, *Phys.Rep.* **2002**, *361*, 57.
[3] J. W. M. Bush, D. L. Hu, *Annu. Rev. Fluid Mech.* **2006**, *38*, 339.
[4] S.-H. Hsu, K. Woan, W. Sigmund, *Mater. Sci. Eng. R* **2011**, *72*, 189.
[5] M. K. Kwak, H.-E. Jeong, T.-I. Kim, H. Yoon, K. Y. Suh, *Soft Matter* **2010**, *6*, 1849.
[6] I. R. Epstein, J. A. Pojman, *An Introduction to Nonlinear Chemical Dynamics: Oscillations, Waves, Patterns, and Chaos*, Oxford University Press, New York **1998**.
[7] B. P. Belousov, in *Collection of Short Papers on Radiation Medicine for 1958*, Med. Publ., Moscow, **1959**, 145.
[8] A. N. Zaikin, A. M. Zhabotinsky, *Nature* **1970**, *225*, 535.
[9] K. Zimmermann, V. A. Naletova, I. Zeidis, V. A. Turkov, E. Kolev, M. V. Lukashevich, G. V. Stepanov, *J. Magn. Magn. Mater.* **2007**, *311*, 450.
[10] S. C. Glotzer, M. J. Solomon, *Nat. Mater.* **2007**, *6*, 557.
[11] P. Akcora, H. Liu, S. K. Kumar, J. Moll, Y. Li, B. C. Benicewicz, L. S. Schadler, D. Acehan, A. Z. Panagiotopoulos, V. Pryamitsyn, V. Ganesan, J. Ilavsky, P. Thiyagarajan, R. H. Colby, J. F. Douglas, *Nat. Mater.* **2009**, *8*, 354.
[12] S. Daniel, M. K. Chaudhury, P.-G. de Gennes, *Langmuir* **2005**, *21*, 4240.
[13] J. G. Ok, S. H. Tawfick, K. A. Juggernauth, K. Sun, Y. Zhang, A. J. Hart, *Adv. Funct. Mater.* **2010**, *20*, 2470.
[14] a) S. Boduroglu, M. Cetinkaya, W. J. Dressick, A. Singh, M. C. Demirel, *Langmuir* **2007**, *23*, 11391; b) M. C. Demirel, *Colloids Surf. A* **2008**, *321*, 121.
[15] E. M. Purcell, *Am. J. Phys* **1977**, *45*, 3.
[16] W. Federle, *J. Exp. Biol.* **2006**, *209*, 2611.
[17] T. Eisner, D. J. Aneshansley, *Proc. Natl. Acad. Sci. USA* **2000**, *97*, 6568.
[18] K. Autumn, Y. A. Liang, S. T. Hsieh, W. Zesch, W. P. Chan, T. W. Kenny, R. Fearing, R. J. Full, *Nature* **2000**, *405*, 681.
[19] Y. Zheng, H. Bai, Z. Huang, X. Tian, F.-Q. Nie, Y. Zhao, J. Zhai, L. Jiang, *Nature* **2010**, *463*, 640.
[20] M. Prakash, J. W. M. Bush, *Int. J. Nonlinear Mech.* **2011**, *46*, 607.
[21] X. Gao, L. Jiang, *Nature* **2004**, *432*, 36.
[22] Y. Zheng, X. F. Gao, L. Jiang, *Soft Matter* **2007**, *3*, 178.
[23] H. F. Bohn, W. Federle, *Proc. Natl. Acad. Sci. USA* **2004**, *101*, 14138.
[24] I. M. Kulic, M. Mani, H. Mohrbach, R. Thaokar, L. Mahadevan, *Proc. R. Soc. B* **2009**, *276*, 2243.
[25] K. Autumn, M. Sitti, Y. A. Liang, A. M. Peattie, W. R. Hansen, S. Sponberg, T. W. Kenny, R. Fearing, J. N. Israelachvili, R. J. Full, *Proc. Natl. Acad. Sci. USA* **2002**, *99*, 12252.
[26] M. Kamperman, E. Kroner, A. del Campo, R. M. McMeeking, E. Arzt, *Adv. Eng. Mater.* **2010**, *12*, 335.
[27] E. Arzt, S. Gorb, R. Spolenak, *Proc. Natl. Acad. Sci. USA* **2003**, *100*, 10603.
[28] J.-H. Dirks, W. Federle, *Soft Matter* **2011**, *7*, 11047.
[29] X. Q. Feng, X. Gao, Z. Wu, L. Jiang, Q. S. Zheng, *Langmuir* **2007**, *23*, 4892.
[30] J. W. M. Bush, M. Prakash, D. L. Hu, *Adv. Insect Physiol.* **2007**, *34*, 117.
[31] a) D. Wu, J.-N. Wang, S.-Z. Wu, Q.-D. Chen, S. Zhao, H. Zhang, H.-B. Sun, L. Jiang, *Adv. Funct. Mater.* **2011**, *21*, 2927; b) J. Gao, Y. Liu, H. Xu, Z. Wang, X. Zhang, *Langmuir* **2010**, *26*, 9673; c) G. Fraenkel, F. Fallil, K. S. Kumarasinghe, *Entomol. Exp. Appl.* **1981**, *29*, 147.
[32] Y.-C. Chung, G.-Y. Hess, F.-W. Yeh, H.-C. Han, C.-Y. Chen, C.-J. Lee, H.-J. Sheen, L.-J. Yang, *J. Micro/Nanolithogr. MEMS MOEMS* **2010**, *9*, 13035.
[33] A. Shastry, M. J. Case, K. F. Böhringer, *Langmuir* **2006**, *22*, 6161.
[34] O. Sandre, L. Gorre-Talini, A. Ajdari, J. Prost, P. Silberzan, *Phys. Rev. E* **1999**, *60*, 2964.
[35] J. G. Leidenfrost, *De Aquae Communis Nonnullis Qualitatibus Tractatus*, Duisburg **1756**.
[36] G. Lagubeau, M. Le Merrer, C. Clanet, D. Quéré, *Nat. Phys.* **2011**, *7*, 395.
[37] V. Jokinen, M. Leinikka, S. Franssila, *Adv. Mater.* **2009**, *21*, 4835.
[38] N. A. Malvadkar, M. J. Hancock, K. Sekeroglu, W. J. Dressick, M. C. Demirel, *Nat. Mater.* **2010**, *9*, 1023.
[39] R. Spohr, G. Sharma, P. Forsberg, M. Karlsson, A. Hallen, L. Westerberg, *Langmuir* **2010**, *26*, 6790.
[40] T.-I. Kim, K. Y. Suh, *Soft Matter* **2009**, *5*, 4131.
[41] K.-H. Chu, R. Xiao, E. N. Wang, *Nat. Mater.* **2010**, *9*, 413.
[42] A. Parness, D. Soto, N. Esparza, N. Gravish, M. Wilkinson, K. Autumn, M. Cutkosky, *J. R. Soc. Interface* **2009**, *6*, 1223.
[43] J. Lee, R. S. Fearing, K. Komvopoulos, *Appl. Phys. Lett.* **2008**, *93*, 191910.
[44] H. E. Jeong, J.-K. Lee, H. N. Kim, S. H. Moon, K. Y. Suh, *Proc. Natl. Acad. Sci. USA* **2009**, *106*, 5639.
[45] C. Kettner, P. Reimann, P. Hänggi, F. Müller, *Phys. Rev. E* **2000**, *61*, 312.
[46] a) M. Cetinkaya, N. Malvadkar, M. C. Demirel, *J. Polym. Sci. Part B: Polym. Phys.* **2008**, *46*, 640; b) M. C. Demirel, S. Boduroglu, M. Cetinkaya, A. Lakhtakia, *Langmuir* **2007**, *23*, 5861.
[47] K. Sekeroglu, U. A. Gurkan, U. Demirci, M. C. Demirel, *Appl. Phys. Lett.* **2011**, *99*, 063703.
[48] L. Mahadevan, S. Daniel, M. K. Chaudhury, *Proc. Natl. Acad. Sci. USA* **2004**, *101*, 23.
[49] C. Christophis, K. Sekeroglu, G. Demirel, I. Thome, M. Grunze, M. C. Demirel, A. Rosenhahn, *Biointerphases* **2011**, *6*, 158.
[50] G. Mahmud, C. J. Campbell, K. J. M. Bishop, Y. A. Komarova, O. Chaga, S. Soh, S. Huda, K. Kandere-Grzybowska, B. A. Grzybowski, *Nat. Phys.* **2009**, *5*, 606.
[51] E. So, M. C. Demirel, K. J. Wahl, *J. Phys. D Appl. Phys.* **2010**, *43*, 045403.
[52] A. A. Darhuber, S. M. Troian, S. M. Miller, S. Wagner, *J. Appl. Phys.* **2000**, *87*, 7768.
[53] B. Zhao, J. S. Moore, D. J. Beebe, *Science* **2001**, *291*, 1023.
[54] C. Lv, C. Yang, P. Hao, F. He, Q. Zheng, *Langmuir* **2010**, *26*, 8704.
[55] L. Mahadevan, Y. Pomeau, *Phys. Fluids* **1999**, *11*, 2449.
[56] D. Richard, D. Quéré, *Europhys. Lett.* **1999**, *48*, 286.
[57] a) D. Bartolo, F. Bouamrirene, É. Verneuil, A. Buguin, P. Silberzan, S. Moulinet, *Europhys. Lett.* **2006**, *74*, 299; b) M. Reyssat, A. Pépin, F. Marty, Y. Chen, D. Quéré, *Europhys. Lett.* **2006**, *74*, 306.
[58] a) N. Malvadkar, S. Park, M. Urquidi-MacDonald, H. Wang, M. C. Demirel, *J. Power Sources* **2008**, *182*, 323; b) N. A. Malvadkar, K. Sekeroglu, W. J. Dressick, M. C. Demirel, *J. Power Sources* **2011**, *196*, 8553.
[59] N. A. Malvadkar, K. Sekeroglu, W. J. Dressick, M. C. Demirel, *Langmuir* **2010**, *26*, 4382.
[60] a) J. Huang, M. Juszkiewicz, W. H. de Jeu, E. Cerda, T. Emrick, N. Menon, T. P. Russel, *Science* **2007**, *317*, 650; b) C. Py, P. Reverdy, L. Doppler, J. Bico, B. Roman, C. N. Baroud, *Phys. Fluids* **2007**, *19*, 91104.
[61] C. Py, P. Reverdy, L. Doppler, J. Bico, B. Roman, C. N. Baroud, *Phys. Rev. Lett.* **2007**, *98*, 156103.
[62] R. E. Newnham, *Properties of Materials: Anisotropy, Symmetry, Structure*, Oxford University Press, Oxford, UK **2005**.

[63] a) M. C. Demirel, A. P. Kuprat, D. C. George, A. D. Rollett, *Phys. Rev. Lett.* **2003**, *90*, 016106; b) A. Kuprat, D. George, G. Straub, M. C. Demirel, *Comp. Mater. Sci.* **2003**, *28*, 199.
[64] A. R. Atilgan, S. R. Durell, R. L. Jernigan, M. C. Demirel, O. Keskin, I. Bahar, *Biophys. J.* **2001**, *80*, 505.
[65] H. Yao, H. Gao, *J. Mech. Phys. Solids* **2006**, *54*, 1120.
[66] a) H. Gao, H. Yao, *Proc. Natl. Acad. Sci. USA* **2004**, *101*, 7851; b) H. Gao, X. Wang, H. Yao, S. Gorb, E. Arzt, *Mech. Mater.* **2005**, *37*, 275; c) B. N. J. Persson, *J. Chem. Phys.* **2003**, *118*, 7614; d) R. Spolenak, S. Gorb, H. Gao, E. Arzt, *Proc. R. Soc. A - Math. Phy.* **2005**, *461*, 305; e) G. Huber, S. N. Gorb, R. Spolenak, E. Arzt, *Biol. Lett.* **2005**, *1*, 2.
[67] P.-G. de Gennes, *Rev. Mod. Phys.* **1985**, *57*, 827.
[68] P.-G. de Gennes, F. Brochard-Wyart, D. Quéré, *Capillarity and Wetting Phenomena: Drops, Bubbles, Pearls, Waves*, Springer, Berlin **2003**.
[69] a) A. W. Adamson, *Physical Chemistry of Surfaces*, Wiley, New York **1982**; b) E. B. Dussan V, *Ann. Rev. Fluid Mech.* **1979**, *11*, 371.
[70] C. W. Extrand, *Langmuir* **2007**, *23*, 1867.
[71] A. C. Balazs, J. M. Yeomans, *Soft Matter* **2010**, *6*, 703.
[72] T. Young, *Phil. Trans. R. Soc. London A* **1805**, *95*, 65.
[73] a) R. E. Johnson, R. H. Dettre, in *Advances in Chemistry Series*, Vol. *43*: *Contact Angle, Wettability, and Adhesion,* (Ed. F. M. Fowkes), American Chemical Society, Washington, DC **1964**, 112; b) R. H. Dettre, R. E. Johnson, in *Advances in Chemistry Series*, Vol. *43*: *Contact Angle, Wettability, and Adhesion,* (Ed. F. M. Fowkes), American Chemical Society, Washington, DC **1964**, *136*; c) R. H. Dettre, R. E. Johnson, *J. Phys. Chem.* **1965**, *69*, 1507.
[74] a) E. B. Dussan V, R. T. P. Chow, *J. Fluid Mech.* **1983**, *137*, 1; b) C. W. Extrand, Y. Kumagai, *J. Colloid Interface Sci.* **1995**, *170*, 515.
[75] G. D. Nadkarni, S. Garoff, *Europhys. Lett.* **1992**, *20*, 523.
[76] R. N. Wenzel, *Ind. Eng. Chem.* **1936**, *28*, 988.
[77] a) A. B. D. Cassie, S. Baxter, *Trans. Faraday Soc.* **1944**, *40*, 546; b) A. B. D. Cassie, S. Baxter, *Nature* **1945**, *155*, 21.
[78] M. Krasowska, R. Krastev, M. Rogalski, K. Malysa, *Langmuir* **2007**, *23*, 549.
[79] A. Checco, T. Hofmann, E. DiMasi, C. T. Black, B. M. Ocko, *Nano Lett.* **2010**, *10*, 1354.
[80] M. Mao, J. Zhang, R. H. Yoon, W. A. Ducker, *Langmuir* **2004**, *20*, 1843.
[81] C. W. Extrand, *Langmuir* **2002**, *18*, 7991.
[82] F. Brochard, *Langmuir* **1989**, *5*, 432.
[83] M. Nosonovsky, *Langmuir* **2007**, *23*, 3157.
[84] J. F. Joanny, P. G. de Gennes, *J. Chem. Phys.* **1984**, *81*, 552.
[85] Y. Pomeau, J. Vannimenus, *J. Colloid Interface Sci.* **1985**, *104*, 477.
[86] M. Reyssat, D. Quéré, *J. Phys. Chem. B* **2009**, *113*, 3906.
[87] a) L. Gao, T. J. McCarthy, *Langmuir* **2006**, *22*, 2966; b) C. Dorrer, J. Rühe, *Langmuir* **2006**, *22*, 7652.
[88] D. J. Acheson, *Elementary Fluid Dynamics*, Oxford University Press, Oxford, UK **1990**.
[89] K. A. Brakke, *Exp. Math.* **1992**, *1*, 141.
[90] a) S. Brandon, A. Wachs, A. Marmur, *J. Colloid Interface Sci.* **1997**, *191*, 110; b) H. Gau, S. Herminghaus, P. Lenz, R. Lipowsky, *Science* **1999**, *283*, 46; c) A. A. Darhuber, S. M. Troian, J. M. Davis, S. M. Miller, S. Wagner, *J. Appl. Phys.* **2000**, *88*, 5119; d) M. Brinkmann, R. Lipowsky, *J. Appl. Phys.* **2002**, *92*, 4296; e) S. Brandon, N. Haimovich, E. Yeger, A. Marmur, *J. Colloid Interface Sci.* **2003**, *263*, 237.
[91] F. J. M. Ruiz-Cabello, H. Kusumaatmaja, M. A. Rodríguez-Valverde, J. Yeomans, M. A. Cabrerizo-Vílchez, *Langmuir* **2009**, *25*, 8357.
[92] Y. Kwon, S. Choi, N. Anantharaju, J. Lee, M. V. Panchagnula, N. A. Patankar, *Langmuir* **2010**, *26*, 17528.
[93] Y. Chen, B. He, J. Lee, N. A. Patankar, *J. Colloid Interface Sci.* **2005**, *281*, 458.
[94] C. Dorrer, J. Rühe, *Langmuir* **2007**, *23*, 3179.
[95] a) C. Dorrer, J. Rühe, *Langmuir* **2007**, *23*, 3820; b) S. Moulinet, D. Bartolo, *Eur. Phys. J. E* **2007**, *24*, 251.
[96] C. Dorrer, J. Rühe, *Langmuir* **2008**, *24*, 1959.
[97] W. Choi, A. Tuteja, J. M. Mabry, R. E. Cohen, G. H. McKinley, *J. Colloid Interface Sci.* **2009**, *339*, 208.
[98] a) M. Bienia, C. Quilliet, M. Vallade, *Langmuir* **2003**, *19*, 9328; b) A. Klingner, J. Buehrle, F. Mugele, *Langmuir* **2004**, *20*, 6770.
[99] M. L. Blow, H. Kusumaatmaja, J. M. Yeomans, *J. Phys.–Condens. Mater.* **2009**, *21*, 464125.
[100] J. Hyväluoma, A. Koponen, P. Raiskinmäki, J. Timonen, *Eur. Phys. J. E* **2007**, *23*, 289.
[101] B. M. Mognetti, H. Kusumaatmaja, J. M. Yeomans, *Faraday Discuss.* **2010**, *146*, 153.
[102] a) W. Jin, J. Koplik, J. R. Banavar, *Phys. Rev. Lett.* **1997**, *78*, 1520; b) P. Collet, J. De Coninck, F. Dunlop, A. Regnard, *Phys. Rev. Lett.* **1997**, *79*, 3704; c) M. Lundgren, N. L. Allan, T. Cosgrove, *Langmuir* **2006**, *23*, 1187.
[103] a) K. Luo, M.-P. Kuittu, C. Tong, S. Majaniemi, T. Ala-Nissila, *J. Chem. Phys.* **2005**, *123*, 194702; b) S. Vedantam, M. V. Panchagnula, *Phys. Rev. Lett.* **2007**, *99*, 176102; c) S. Vedantam, M. V. Panchagnula, *J. Colloid Interface Sci.* **2008**, *321*, 393.
[104] a) M. Do-Quang, G. Amberg, *Math. Comput. Simulat.* **2010**, *80*, 1664; b) M. Do-Quang, G. Amberg, *Phys. Fluids* **2009**, *21*, 022102.
[105] a) D. M. Anderson, G. B. McFadden, A. A. Wheeler, *Ann. Rev. Fluid Mech.* **1998**, *30*, 139; b) D. Jacqmin, *J. Fluid Mech.* **2000**, *402*, 57; c) H.-B. Nguyen, J.-C. Chen, *Phys. Fluids* **2010**, *22*, 062102; d) R. Scardovelli, S. Zaleski, *Ann. Rev. Fluid Mech.* **1999**, *31*, 567; e) A. K. Das, P. K. Das, *Langmuir* **2010**, *26*, 9547.
[106] A. Fakhari, M. H. Rahimian, *Phys. Rev. E* **2010**, *81*, 036707.
[107] H. Kusumaatmaja, J. M. Yeomans, in *Simulating Complex Systems by Cellular Automata*, (Eds: A. G. Hoekstra, J. Kroc, P. M. A. Sloot), Springer-Verlag, Berlin **2010**, 241.
[108] O. Kuksenok, D. Jasnow, J. Yeomans, A. C. Balazs, *Phys. Rev. Lett.* **2003**, *91*, 108303.
[109] H. Kusumaatmaja, M. L. Blow, A. Dupuis, J. M. Yeomans, *Europhys. Lett.* **2008**, *81*, 36003.
[110] B. M. Mognetti, J. M. Yeomans, *Phys. Rev. E* **2009**, *80*, 056309.
[111] D. L. Hu, J. W. M. Bush, *Nature* **2005**, *437*, 733.
[112] G. Ince, K. K. Gleason, M. C. Demirel, *Soft Matter* **2011**, *7*, 638
[113] W. J. Dressick, L. M. Kondracki, M.-S. Chen, S. L. Brandow, E. Matijević, J. M. Calvert, *Colloids Surf. A* **1996**, *108*, 101.